

1 **Biotrophic interactions disentangled: In-situ localisation of mRNAs to decipher plant and**
2 **algal pathogen – host interactions at single cell level.**

3

4 Julia Badstöber¹, Claire M. M. Gachon², Adolf M. Sandbichler³, Sigrid Neuhauser¹

5

6 ¹Institute of Microbiology, University of Innsbruck, A-6020 Innsbruck, Austria

7 ²The Scottish Association for Marine Science, Scottish Marine Institute, Oban PA37 1QA, UK

8 ³Institute of Zoology, University of Innsbruck, A-6020 Innsbruck, Austria

9

10 Author for correspondence:

11 *Sigrid Neuhauser*

12 *Tel: +43 (0) 512 507-51259*

13 *Email: Sigrid.Neuhauser@uibk.ac.at*

14

15

16 **Summary**

17

18 Plant-pathogen interactions follow spatial and temporal developmental dynamics where gene
19 expression in pathogen and host undergo crucial changes. Therefore, it is of great interest to
20 detect, quantify and localise where and when key genes are active to understand these processes.
21 Many pathosystems are not accessible for genetic amendments or other spatially-resolved gene
22 expression monitoring methods. Here, we adapt single molecule FISH techniques to
23 demonstrate the presence and activity of mRNAs at the single-cell level using phytomyxids in
24 their plant and algal host in lab and field material. This allowed us to monitor and quantify the
25 expression of genes from the clubroot pathogen *Plasmodiophora brassicae*, several species of
26 its *Brassica* hosts, and of several brown algae, including the genome model *Ectocarpus*
27 *siliculosus*, infected with the phytomyxid *Maullinia ectocarpii*. We show that mRNAs are
28 localised along a spatiotemporal gradient, thus providing a proof-of-concept of the usefulness
29 of single-molecule FISH to increase knowledge about the interactions between plants, algae
30 and phytomyxids. The methods used are easily applicable to any interaction between microbes
31 and their algal or plant host, and have therefore the potential to rapidly increase our
32 understanding of key, spatially- and temporally-resolved processes underpinning complex
33 plant-microbe interactions.

34

35 **Key words:** biotroph, mRNA localisation, Phaeophyceae, Phytomyxea, plant pathogen
36 interactions, RCA FISH, single cell biology, single molecule FISH.

37

38 Introduction

39

40 Thanks to a series of technological advances over the last years, it has become clear that many
41 biological processes within and between organisms are best studied at the single cell level (e.g.
42 Libault *et al.*, 2017; Moor & Itzkovitz, 2017). Single cell approaches provide a revolutionary
43 toolset to study interactions, especially the complex intermingled crosstalk between biotrophic
44 pathogens and their algal or plant hosts. Biotrophs keep their host's cells alive during their
45 development and growth and, therefore, have evolved a multitude of strategies to escape
46 detection but to still obtain nutrients or water from their host (Kemen & Jones, 2012; Zeilinger
47 *et al.*, 2016). In such interactions, timing is crucial: the pathogen first needs to escape the host
48 defence while establishing itself, but in a subsequent step the pathogen and host communicate
49 about nutrients to be exchanged. Hence, gene expression changes rapidly at the cellular level,
50 and can differ between neighbouring cells (Buxbaum *et al.*, 2015). Unless they are combined
51 with expensive or time-consuming techniques such as laser-assisted microdissection, widely
52 used methods such as qPCR or RNAseq are not able to account for spatial and temporal
53 heterogeneity between the cells, and therefore are impracticable to study single-cell changes at
54 the scale of organs or macro-organisms. On the other hand, transformation or genetic
55 manipulation remains inaccessible for a wide range of pathogens or hosts, especially those that
56 cannot be grown in the lab and/or for which only very limited genetic information is available
57 (Libault *et al.*, 2017). Furthermore, current work on plant and algal microbiomes makes
58 increasingly clear that functional studies require to take into account complex microbial
59 communities which include a huge diversity of „non-model“ organisms, many of which are not
60 accessible to culturing or genome amendment techniques (Egan *et al.*, 2013;
61 Vandenkoornhuys *et al.*, 2015; Müller *et al.*, 2016). Thus, descriptive approaches such as FISH
62 (Fluorescence In Situ Hybridisation) have a renewed potential to start exploring these
63 communities functionally.

64 Indeed, most single-cell approaches available currently lack the potential to be used routinely
65 outside of model organisms to study the dynamic transcriptomic changes of single cells. One
66 notable exception is the *in situ* localisation of individual mRNAs via FISH (Wang & Bodovitz,
67 2010; Misra *et al.*, 2014; Libault *et al.*, 2017). FISH techniques have been utilised to study gene
68 expression patterns and the distribution of mRNA genes in human cell lines (Weibrecht, I *et*
69 *al.*, 2013), different animal models (e.g. Trcek *et al.*, 2017), fungi and yeasts (e.g. Niessing *et*
70 *al.*, 2018) and plants (Bruno *et al.*, 2011; Duncan *et al.*, 2016b; Francoz *et al.*, 2016). Recent
71 improvements involving fluorophores, microscopic detection and resolution now allow to
72 localise individual mRNAs of interest (Buxbaum *et al.*, 2015). Patterns of mRNA expression
73 and the subcellular organisation of mRNAs can thus be accessed. Ultimately this leads to a
74 better understanding of the regulatory processes behind the translation of genetic information
75 (Chen *et al.*, 2015), without requiring genetic manipulation of the organism of interest, nor the
76 availability of extensive genetic and molecular data. Additionally, this can be applied to field-
77 collected samples, which opens new research lines for uncultivable organisms once an mRNA
78 sequence of interest is available.

79 Phytophyxea (Rhizaria, Endomyxa) are a group of economically important plant pathogens,
80 including e.g. *Plasmodiophora brassicae*, the clubroot pathogen, causing a loss of roughly 10
81 % of the world brassica crop production (Schwelm *et al.*, 2018). Additionally, ten phytomyxid

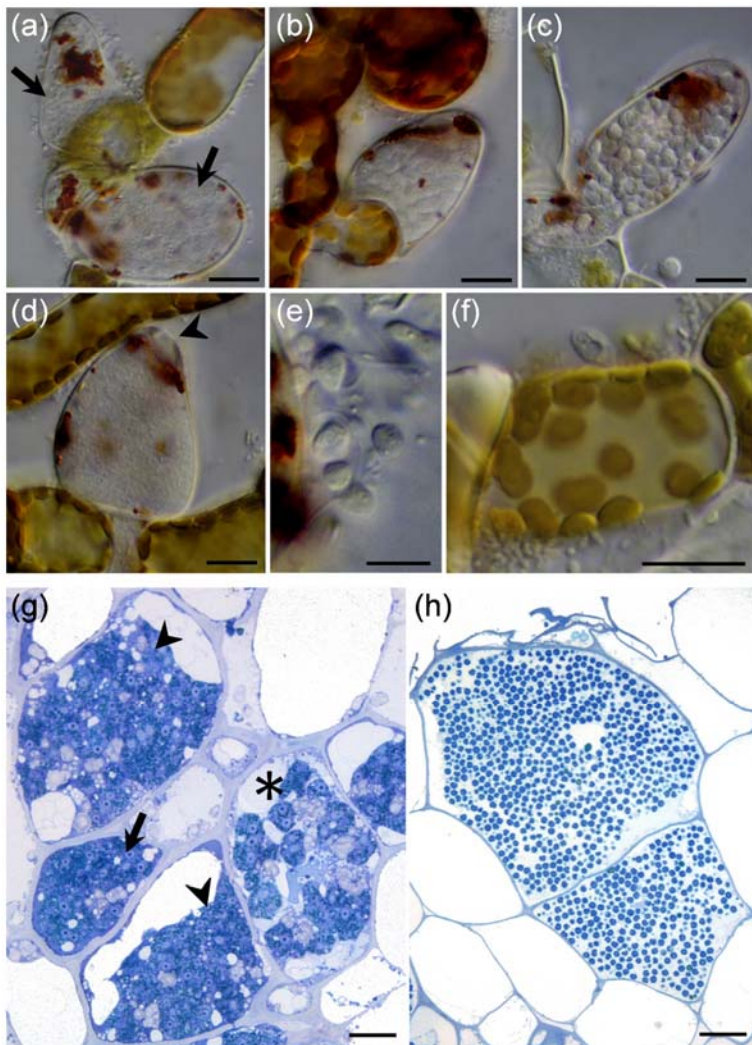
82 species parasitize important marine primary producers, namely brown algae, seagrasses and
83 diatoms, with essentially unknown ecological consequences (Neuhauser *et al.*, 2011; Murúa *et*
84 *al.*, 2017). In brown algae, the galls formed by *Maullinia braseltonii* on the Pacific bull kelp
85 (*Durvillea antarctica*) affect the commercial value of this locally important food source. Its
86 closely related parasite, *Maullinia ectocarpii*, infects a broad range of filamentous algae
87 spanning at least four orders, including the genome model *Ectocarpus siliculosus* and
88 gametophytes of the giant kelp *Macrocystis pyrifera* (Maier *et al.*, 2000). Its availability in
89 laboratory culture makes it a good model to start deciphering the interaction between
90 phytomyxids and their marine hosts.

91 Despite their importance as plant and algal pathogens, Phytomyxea have been difficult to study,
92 mostly because they cannot be cultured without their host and because they have a complex
93 multi-stage life cycle (Schwelm *et al.*, 2018). This life cycle comprises two functionally
94 different types of heterokont zoospores (primary and secondary), multinucleate plasmodia
95 (sporangial and sporogenic), zoosporangia and resting spores. Primary zoospores (Fig. 1e)
96 infect suitable hosts (Fig. 1f) and develop into multinucleate sporangial plasmodia (Fig. 1a)
97 which mature (Fig. 1b, 1c) and release primary or secondary zoospores. This sporangial part of
98 the life cycle is often restricted to few host cells. Secondary zoospores develop into
99 multinucleate sporogenic plasmodia (Fig. 1g) which can grow to considerable size inside of the
100 host, which in some species results in the typical hypertrophies. The sporogenic part of the life
101 cycle ends in the formation of the resistant resting spores (Fig. 1h). Resting spores are passively
102 released from the disintegrating host tissue and can persist for decades in the environment.

103 Genome and transcriptome data became available only recently for *P. brassicae* (Schwelm *et*
104 *al.*, 2015; Rolfe *et al.*, 2016). Yet the unavailability of genetic manipulation of the parasite
105 forces all functional studies to be conducted on transformed plant hosts (mainly *A. thaliana*)
106 either focussing on the host side of the response (e.g. Irani *et al.*, 2018) or by overexpressing *P.*
107 *brassicae* genes in the host (Bulman *et al.*, 2018) or in other plant pathogenic fungi (Singh *et*
108 *al.*, 2018). Likewise, genome resources are available for brown algae (Ye *et al.*, 2015; Cormier
109 *et al.*, 2016), but this group yet remains inaccessible to transformation, genome editing or
110 RNAi, to the exception of *Fucus* zygotes (Farnham *et al.*, 2013). Apart from taxonomic
111 markers, no molecular information is currently available for *Maullinia ectocarpii* or any other
112 marine phytomyxid. In this context, the prospect of monitoring gene expression of
113 phytomyxean parasites in their host, linking the expression of selected genes to specific stages
114 of the life cycle and to specific time points in the development of the pathogen, is to get a better
115 understanding of the interaction.

116 Here, we developed tools to monitor gene expression of intracellular pathogens and to monitor
117 the response of their hosts (plants and brown algae) upon infection. For this purpose, two
118 different approaches of single molecule mRNA localisation were evaluated: smFISH (single
119 molecule FISH), which is based on a series of fluorescently labelled probes that tile along the
120 mRNA of interest (Duncan *et al.*, 2016b) and RCA-FISH (Rolling Circle Amplification-FISH),
121 which is based on in-situ transcription of RNA followed by in-situ-RCA signal amplification
122 (Weibrecht, Irene *et al.*, 2013). Genes were selected on the basis of available biological
123 background, to allow to not only test and validate FISH methods, but to also validate the
124 feasibility and usefulness of these methods to disentangle biological information. The following
125 *P. brassicae* genes were selected (i) the housekeeping gene Actin1 (GenBank: AY452179.1)

126 (Archibald & Keeling, 2004) (ii) a SABATH-type methyltransferase from *P. brassicae*
127 upregulated during the later stages of pathogen development (PbBSMT, GenBank:
128 JN106050.1, (Ludwig-Muller et al., 2015), which is able to methylate salicylic acid (SA),
129 benzoic and anthranilic acids. To monitor mRNA expression and localisation in the host, the
130 following genes were tested: (i) the *Brassica rapa* maltose excess protein 1 (MEX1, GenBank:
131 XM_009109278.2) that encodes a maltose transporter, and (ii) the vanadium-dependent
132 bromoperoxidase (vBPO) of *Ectocarpus siliculosus* Ec32m (Genbank: CBN73942.1), a stress-
133 inducible enzyme assumed to halogenate defensive secondary metabolites (Leblanc *et al.*, 2015;
134 Strittmatter *et al.*, 2016).
135



136
137 **Figure 1: Phytomyxid Morphology.** Sporangial life cycle of *Maullinia ectocarpii* (a-f) and sporogonic development
138 of *P. brassicae* (g-h). a-f: *Maullinia ectocarpii* infecting filaments of the brown algae *Macrocystis pyrifera*. Pale
139 cells are filled with the parasite. (a) sporangial plasmodia in enlarged algal cells (arrows). (b) sporangial
140 plasmodium transitioning to form a zoosporangium. (c) mature zoosporangium filled with zoospores. (d) empty
141 sporangium after the primary zoospores were released through an apical opening (arrowhead). (e) primary
142 zoospores with two anterior flagella. (f) primary zoospore infecting the algal filament. (g, h) Chinese cabbage
143 clubroots, cross section, methyleneblue staining (g) multinucleate, sporangial plasmodia in different
144 developmental stages. Actively growing, sporogonic plasmodia (arrow, arrowheads) and one plasmodium
145 showing the typical lobose structure (asterisk). (h) *P. brassicae* resting spores. All resting spores inside of one
146 host cell were formed from the same sporogonic plasmodium. Bars 10 μm .

147

148 **MATERIAL AND METHODS**

149

150 **Preparation and storage of the biological material**

151

152 Clubroot-infected Brassica plants

153

154 Field sampling

155 Clubroot infected white cabbage (*Brassica oleracea* var. *capitata* f. *alba*), broccoli (*Brassica*
156 *oleracea* var. *italica*), Chinese cabbage (*Brassica rapa* ssp. *pekinensis*) and kohlrabi (*Brassica*
157 *oleracea* var. *gongylodes*) were collected from a commercial field (Ranggen, Austria,
158 47°15'24"N, 11°13'01"E). Clubroots were rinsed with tap water and treated as described below.

159

160 Inoculation and cultivation of plants

161 Chinese cabbage (*Brassica rapa* cv. 'Granaat', European Clubroot Differential Set ECD-05)
162 seeds were germinated on wet tissue paper for three days and then planted in a potting soil
163 mixture (pH ~ 5.7, mixing standard compost, rhododendron soil and sand 4:2:2). Plants were
164 grown with a photoperiod of 12 h. After 12 days, plants were inoculated with 7×10^6 spores of
165 *P. brassicae*. Root galls were harvested after six to seven weeks.

166

167 Sample Fixation and preparation

168 Clubroots were cut into ca. 3 x 4 mm pieces to allow for a more homogenous fixation. Samples
169 were transferred into Histofix 4% (phosphate-buffered formaldehyde solution, Carl Roth)
170 where they remained for 1 - 12 h depending on sample size. Samples were used directly, or
171 were washed in an ascending ethanol series for long-term storage (50 %, 80 %, 2x 96 %; all
172 dilutions made with DEPC [diethyl pyrocarbonate]-treated water) and stored at -20 °C until
173 use.

174 Clubroots (or clubroot pieces) were cut transversal with an RNase free razor blade by hand and
175 washed with 1x PBS buffer (phosphate-buffered saline, 137 mM NaCl, 10 mM phosphate, 2.7
176 mM KCl, DEPC treated water). Making the cuts by hand posed a significantly lower risk of
177 RNase contamination than using a cryotome (Reichert-Jung, Frigocut 2800, Suppl. Note S1).

178

179 Growth and maintenance of *M. ectocarpii* infected *Ectocarpus siliculosus* Ec32m and 180 *Macrocystis pyrifera*

181 *Ectocarpus siliculosus* (fully sequenced genome strain Ec32m, CCAP 1310/4) was infected
182 with *Maullinia ectocarpii* (CCAP 1538/1), using a clonal culture of *Macrocystis pyrifera*
183 female gametophyte (CCAP 1323/1) as an intermediate host, as described by (Strittmatter *et*
184 *al.*, 2016). Cultures were maintained at 15 °C with 12 h photoperiod, 20 micromol photon m⁻²
185 s⁻¹ in artificial seawater (ASW) with half strength modified Provasoli (West & McBride, 1999).
186 Cultures were regularly checked microscopically and samples were harvested and fixed as
187 described above, replacing DEPC-treated water by DEPC-treated ASW. Samples were stored
188 at -20 °C until use.

189

190

191

192 **Single molecule mRNA visualisation**

193

194 To prevent RNase contamination, experiments were done in RNase-free environment with
195 RNase-free reaction mixtures. To avoid photobleaching, the samples were protected from light
196 during and after the hybridisation of the fluorescently labelled oligonucleotides. All enzymes
197 and reaction mixtures were kept on ice during use. Reaction tubes were incubated using a PCR
198 cyclor with heated lid to avoid evaporation or a thermal block. All incubation and amplification
199 steps were performed in 0.2 mL PCR reaction tubes unless otherwise stated.

200

201 RCA-FISH (Rolling circle amplification – Fluorescence in Situ Hybridisation)

202 RCA-FISH is based on the *in-situ* reverse-transcription of mRNA, a subsequent signal
203 amplification using a loop-shaped DNA target probe as starting point for the RCA amplification
204 and followed by FISH detection of the so amplified DNA (Tab. 1) (Weibrecht, I *et al.*, 2013).
205 Experimentally this process can be divided into four steps: (i) Reverse transcription of target
206 mRNAs, using a mRNA specific locked nucleic acid (LNA) primer. (ii) RNase H digestion of
207 the RNA part of the RNA/DNA hybrid sequence, because in all subsequent steps the cDNA
208 generated by the reverse transcription serves as template. (iii) RCA amplification: A so-called
209 padlock probe, which forms a little loop when binding to the cDNA, serves as circular DNA
210 template for RCA. The loop like sequence is amplified and as a part of it a sequence
211 complementary to the detection probe. (iv) Signal detection: A standard FISH probe is used to
212 detect the amplified signal.

213

214 Primer and probe design:

215 LNA-Primer: LNA primers were approximately 25 bp long and located close to the 3' end of
216 the mRNA. Starting from the 5' end of the LNA primer, every second nucleotide was replaced
217 by its LNA counterpart, in total 7 LNAs (Tab. 1).

218 Padlock Probe: About 15bp at each of the 3' and 5' ends of the padlock probe are
219 complementary to the cDNA sequence. When these two regions bind to the cDNA, the central
220 region of the probe (ca. 50 bp) forms a loop, similar to the shackle of a padlock. This central
221 region contains a generic detection sequence (~ 23bp) flanked by random filler sequences (Tab.
222 1). This loop-like structure serves as target for the Phi-Polymerase mediated RCA which is
223 amplifying the detection sequence and consequently the signal. The padlock probe has to be
224 phosphorylated before use. Overall the structure of the padlock probe is: 5' phosphate – **15bp**
225 **complementary to cDNA** – 5-15bp random filler – detection sequence - 5-15bp random filler -
226 **15bp complementary to cDNA** - 3'.

227 Detection Probe: This is a fluorescent, mono-labelled FISH probe complementary to the
228 detection sequence included in the padlock probe.

229 To check the secondary structures in all three types of probes, UNAFold
230 (<https://eu.idtdna.com/UNAFold>) was used. Specificity and potential off-target binding sites
231 were checked by blasting the sequences (<https://blast.ncbi.nlm.nih.gov/>) against the nr database.

232

233

234

235 **Table 1:** RCA-FISH probes. PbBSMT (*GenBank: JN106050.1*) and Actin1 (*GenBank: AY452179.1*)
 236 are genes of *P. brassicae*. LNA modified nucleotides are shown in orange, padlock probe target-specific
 237 parts are shown in italics and bold letters and the detection sequences are shown underlined.

Oligonucleotide	Sequence
PbBSMT (GenBank: JN106050.1)	
LNA primer PbBSMT	5' CCCGTTCACCTGGC ATGACTATTCG 3'
Padlock probe PbBSMT	5' phosphate-- <i>ATAAACTCGAATAGTTCGTTTTATTAGGTC</i> AAATGCTGCTGCTGCTACTACTCTTTAGCGTTCG <i>TTCC</i> 3'
Detection probe PbBSMT	5' Cy3—GGTCAATGTCTGCTGCTGCTACTAC 3'
Actin1 (GenBank: AY452179.1)	
LNA primer Actin1	5' CGTACCAGTCGATC ATGAAGTGCGACG 3'
Padlock probe Actin1	5' phosphate— <i>AGTCGACGTCGC</i> ACTTTGATTACTAGGCCAATGTCCTCAGTACTACTACTCTTACAGGTCCTT <i>GCGGA</i> 3'
Detection probe Actin1	5' Cy3—GGCCAATGTCCTCAGTACTACTAC 3'

238

239 RCA-FISH experimental Method

240 A tick-off style, step-by-step protocol is provided in Suppl. Note S2. Modifications and notes
 241 on filamentous starting material is provided in Suppl. Note S1.

242 Sections from clubroot samples or algal material were transferred into the reaction tubes were
 243 they were rehydrated in PBS-T (0.05% Tween-20 in 1x PBS). Several sections may be treated
 244 in one tube, as long as the material is submerged in the reaction mix. For our samples 50 µl of
 245 reaction mix were required for consistent results. The PBS-T was removed and the reverse
 246 transcription mix (20 U µl⁻¹ RevertAid H minus M-MuLV reverse transcriptase, 1 U µl⁻¹
 247 RiboLock RNase inhibitor, 1x M-MuLV RT buffer, 0.5 mM dNTP, 0.2 µg µl⁻¹ BSA, 1 µM
 248 LNA primer) was added. Samples were incubated for 1 h at 37 °C in a PCR cycler. Samples
 249 were washed twice with PBS-T and were then incubated in 3.7% PFA (paraformaldehyde in 1
 250 x PBS) for 5 min at room temperature. Samples were washed in PBS-T. This was followed by
 251 RNase H digestion, hybridisation and ligation of the padlock probe in the hybridisation mix (1
 252 U µl⁻¹ Ampligase, 0.4 U µl⁻¹ RNase H, 1 U µl⁻¹ RiboLock RNase inhibitor, 1x Ampligase buffer,
 253 0.2 µg µl⁻¹ BSA, 0.05 M KCl, 20% formamide, 0.1 µM padlock probe). Samples were incubated
 254 for 15 min at 45 °C and washed in PBS-T. Rolling circle amplification was done for 45 min at
 255 37 °C (polymerase reaction mix: 1 U µl⁻¹ Phi29 DNA polymerase, 1 U µl⁻¹ RiboLock RNase
 256 inhibitor, 1x Phi29 buffer, 0.25 mM dNTP, 0.2 µg µl⁻¹ BSA, 5% Glycerol), followed by a PBS-
 257 T washing step. The detection probe was hybridised for 10 min at 37 °C in a detection probe
 258 reaction mix (1x hybridisation mix (2x SSC saline-sodium citrate buffer (300 mM sodium
 259 chloride, 30 mM sodium citrate), 40% (vol/vol) formamide, 0.1 µM detection oligonucleotide).
 260 Samples were washed twice with PBS-T. Samples were carefully transferred and arranged on
 261 microscope glass slides, mounted with Vectashield (H-1000, Vector Laboratories) mounting
 262 medium and covered with a coverslip. The coverslips were sealed with clear nail polish and the
 263 slides were imaged using a laser scanning microscope. To exclude the possibility of false
 264 positive signals, control samples were treated without padlock probes.

265

266

267 Single molecule FISH (smFISH)

268 smFISH relies on a large number of mono-labelled DNA-probes complementary to the mRNA
269 sequences of interest. The protocol described here was adapted from (Duncan *et al.*, 2016a).
270 Probes for smFISH were designed and ordered using the Stellaris[®] Probe Designer
271 (<http://singlemoleculfish.com>, all probes labelled with Quasar570) or ordered via
272 <https://biomers.net/> (Cy3 labelled probes). A set of 48 different probes was generated,
273 complementary to our mRNA sequences of interest (PbBSMT GenBank: JN106050.1, vBPO
274 GenBank CBN73942.1, MEX1 GenBank: XM_009109278.2, Suppl. Tab. S1-3). To verify the
275 specificity of the oligonucleotides to the target sequence, the sequences were blasted against
276 the NCBI nr database.

277

278 smFISH experimental method

279 A tick-off style step-by-step protocol is provided in Suppl. Note S3.

280 Samples were washed in 1x PBS buffer and were transferred to 0.2 mL PCR tubes and incubated
281 for 1 h in 70% EtOH at room temperature. The EtOH was removed and samples were washed
282 twice for three minutes in washing buffer (10% formamide, 2x SSC). Samples were then
283 incubated in 50 μ l of hybridisation buffer (100 mg ml⁻¹ dextran sulfate, 40% formamide in 2x
284 SSC, 250 nM probe-mix) in a PCR cycler at 37 °C overnight with the lid heated to 100 °C to
285 prevent evaporation. Subsequently, the hybridisation buffer was removed and the samples were
286 rinsed twice with washing buffer, before being incubated in the washing buffer at 37 °C for 30
287 minutes. Nuclei were counterstained in 50 μ l 4,6-diamidino-2-phenylindole (DAPI) solution
288 (100 ng μ l⁻¹ in washing buffer) for 15 min at 37 °C. Samples were washed in 50 μ l 2x SSC for
289 1 min before being equilibrated in 50 μ l GLOX buffer (0.4% glucose in 10 nM Tris-HCl, 2x
290 SSC) for 3 minutes, followed by 50 μ l GLOX buffer containing enzymes (1% glucose oxidase
291 and 1% catalase in GLOX buffer) after removal. Samples were carefully mounted using
292 tweezers in the GLOX buffer containing enzymes. The mounted samples were sealed with nail
293 polish and imaged as soon as possible to avoid a reduction of image quality.

294 To confirm RNA specificity and to evaluate autofluorescence of the samples, control samples
295 were treated with RNase or were analysed without the addition of smFISH probes. RNase A
296 treatment for sample sections was performed for 1 h at 37 °C (100 μ g ml⁻¹) before the
297 hybridisation step (Supplementary Note S3, between steps 4 and 5). After RNase A digestions
298 the samples were washed twice in 10 mM HCl for 5 min and rinsed twice in 2x SSC for 5 min.
299 These samples were then incubated with the smFISH probes as described above. Quasar570
300 labelled smFISH probes were used with the corresponding Stellaris buffers. Those samples
301 were mounted in Roti-Mount FluorCare (Carl Roth).

302

303 **Image acquisition and data analyses**

304 Images were acquired with a Leica SP5-II confocal laser scanning microscope (CLSM), using
305 the LAS AF software (version 2.7, Leica Microsystems, Germany) and a Zeiss Cell
306 Observer.Z1 Spinning Disk microscope using the ZEN software (Carl Zeiss Microscopy,
307 Germany). The Leica SP5-II CLSM was equipped with a hybrid detector and a 20x (0.7 NA)
308 or 63x (1.3 NA) objective lens and with the following lasers: 405 nm, 458 nm, 514 nm, 561
309 nm, 633 nm. For probes labelled with Cy3 (Actin1, PbBSMT, and vBPO) and Qu570 (MEX1),
310 an excitation of 514 nm was used and the emission was detected at 550 – 585 nm. For DAPI

311 staining, 405 nm excitation was used and emission was detected at 430 – 485 nm. The Zeiss
312 Axio Cell Observer.Z1 was equipped with a CSU-X1 spinning disc confocal using 25x, 40x or
313 63x water-immersion lenses. Images were analysed using ImageJ (Schneider *et al.*, 2012) which
314 was used to generate coloured overlay images of the different emissions recorded and for
315 creating maximum projections of the z-stacks. Resizing and linear brightness and contrast
316 adjustments were performed in GIMP 2.8.22 (www.gimp.org). The original unprocessed
317 images will be deposited at figshare using the final numbering of the figures.

318 For the automated counting of FISH signals in every individual slice of an image stacks a "find
319 stack maxima" macro in Fiji (Schindelin, 2012), a distribution of the free image analysis
320 software Image J, was applied. CLSM settings were defined in advance to record individual
321 signals in 2 consecutive slices to yield full signal coverage (minimum pinhole settings resulting
322 in a slice thickness of 0.85µm; z-stepsize around 0.8 µM or below). Noise tolerance values were
323 evaluated preliminary to best fit the fluorescence signal. Regions of interest (ROI) were marked
324 (Suppl. Fig. S1, S2), measured and saved. Finally, automated counts of every slice in a stack
325 within a ROI were summarised and normalised to volume and corrected for slice number and
326 z-stepsize. Results are presented in FISH signal maxima per µm³.

327

328 **RESULTS**

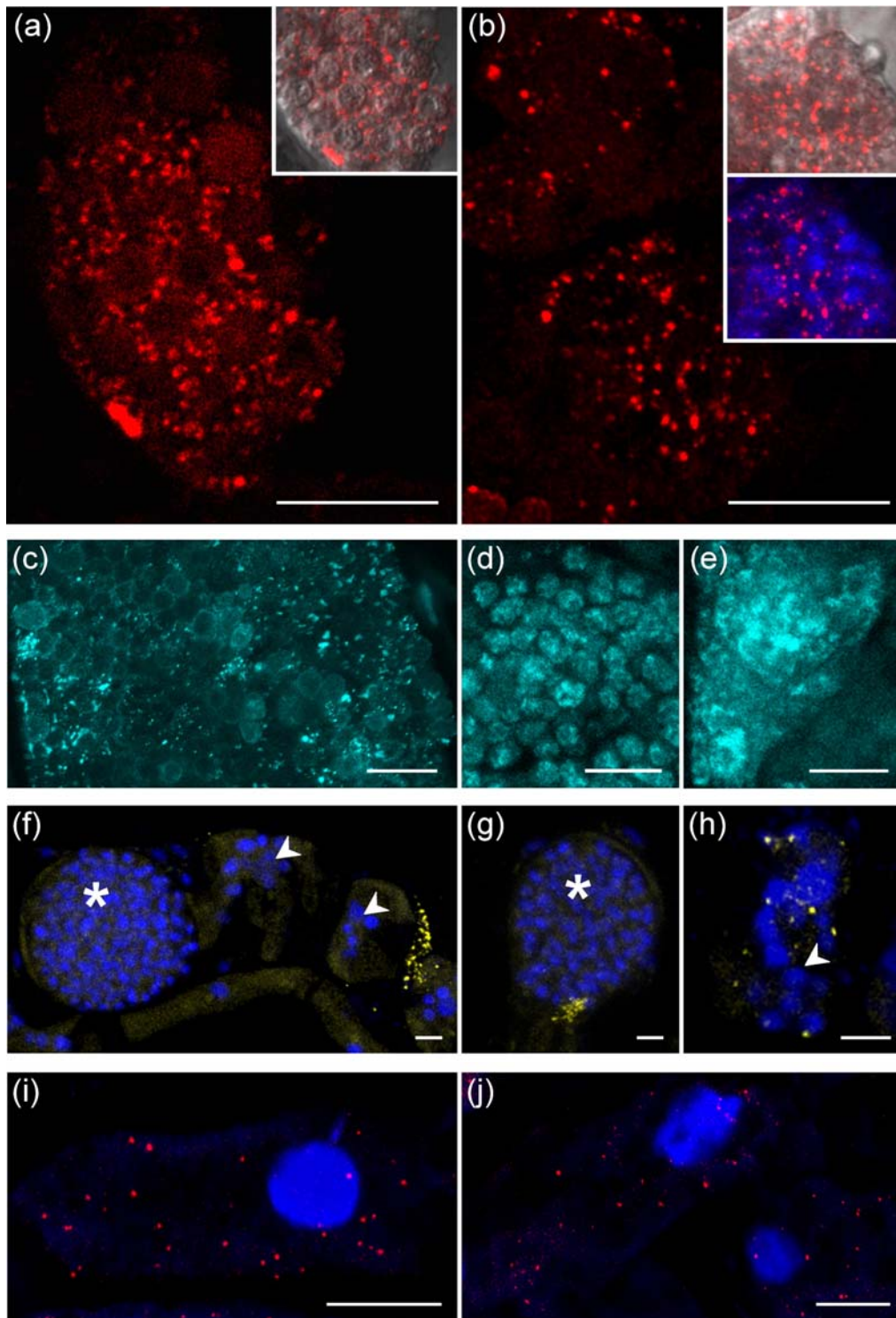
329 Two *P. brassicae* genes were analysed using RCA-FISH: the SABATH-type methyltransferase
330 PbBSMT and Actin1. In contrast to Actin1, a spatiotemporal expression pattern has already
331 been hypothesised for PbBSMT (Ludwig-Muller *et al.*, 2015); thus we also analysed its
332 expression using smFISH to compare the performance of both methods, qualitatively and
333 quantitatively.

334 **Qualitative and quantitative comparison of smFISH and RCA-FISH**

335 Localisation of PbBSMT mRNAs resulted in the same spatio-temporal pattern of dotted signals,
336 when smFISH or RCA-FISH were used (Fig 2 a-b, see details in Suppl. Figs. S1, S2, S3, S5 –
337 S7). In z-stack maximum projections mRNA signals can appear clustered. However, single
338 signals in individual planes appear as dots with sizes ranging from 0.2 to 0.7 µm (Suppl. Fig.
339 S3, Video S1). No signal could be detected in the controls without padlock probe (RCA FISH,
340 Suppl. Fig S4a), after RNase treatment (smFISH, Suppl. Fig. S4b) and in uninfected plant roots
341 (data not shown).

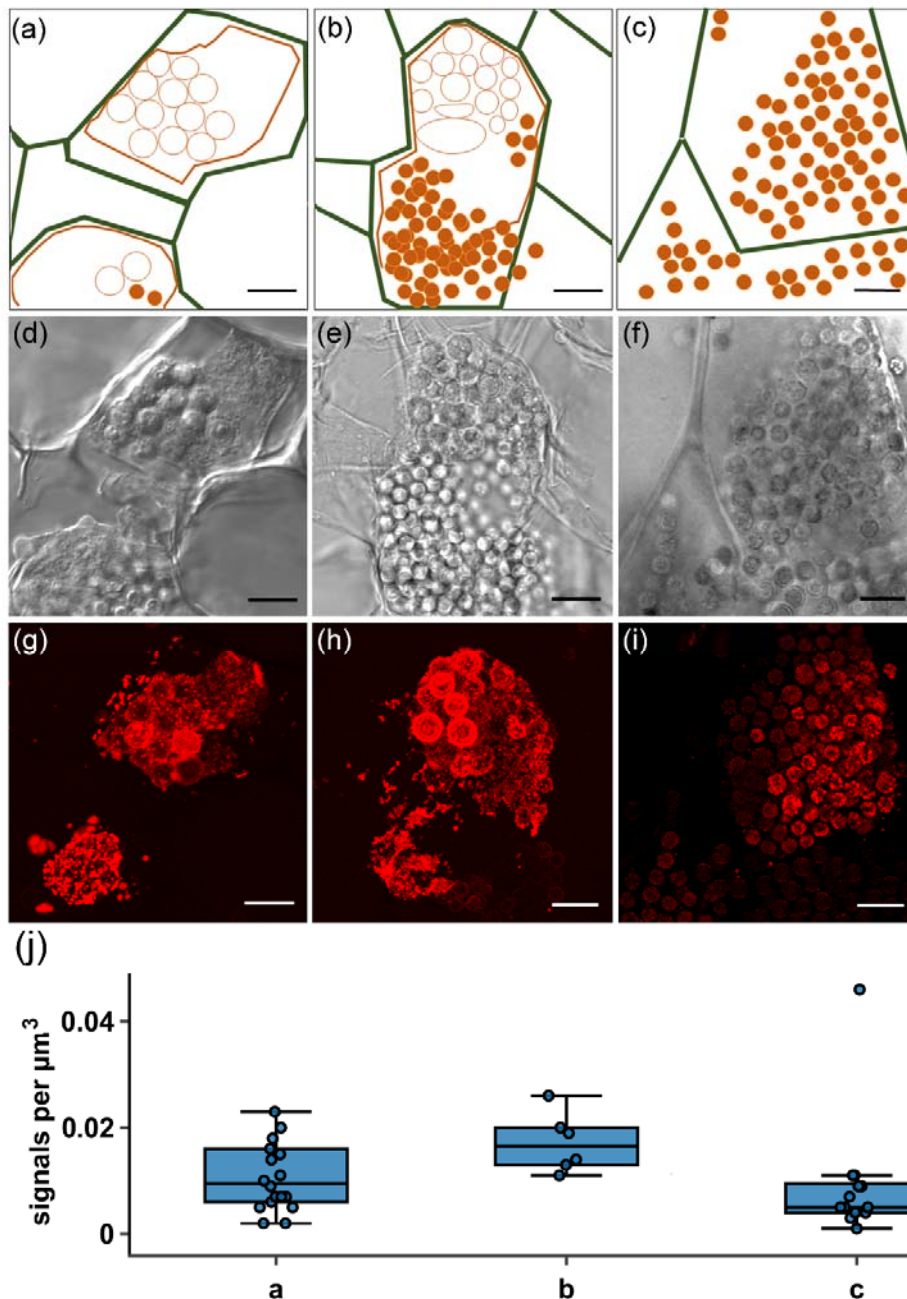
342 The hypothesised spatiotemporal expression pattern of PbBSMT was identified with RCA-
343 FISH (Fig. 3 g, h) and smFISH (Fig. 3i, Suppl. Fig. S7). Specifically, PbBSMT mRNAs started
344 to appear in large quantities once sporogenic plasmodia started to develop into spores (Fig. 3g);
345 the signals appeared dot-like in the individual planes, while in the maximum projection the
346 mRNAs appeared accumulated around the developing spores. With progressing spore
347 formation, the intensity and number of signals intensified around the outside the developing
348 spores, both in individual layers, where most of the signals were still visible as separated dots,
349 and in the maximum projection where mRNA signals appeared to cover the surface of the
350 developing spores (Fig. 3 h, see 3D reconstruction in Suppl. Video S1). Subsequently, the
351 signals became fewer and smaller until they disappeared once the spores were fully developed
352 (Fig. 3 i). This pattern indicates that the presence of PbBSMT or its mRNA plays a role during
353 the transition from plasmodial growth to sporogenesis in *P. brassicae*.

354



355
356 **Figure 2:** mRNA-transcript localisation in *P. brassicae* (a-e, Cy3), *Ectocarpus siliculosus* Ec32m (f-h, Cy3) and
357 *Brassica rapa* (i-j, Qu570). (a) mRNAs of *P. brassicae* PbBSMT, RCA FISH and, (b) smFISH. The plasmodia in (a) and
358 (b) are transitioning from the active growth phase of the plasmodium to resting spore formation, which can be
359 recognised by the round “compartments” visible in the bright field inserts. Multiple nuclei can be seen (b, insert).
360 (c-e): Actin1 mRNAs of *P. brassicae* using RCA FISH (cyan). (c) during the onset of resting spore formation. (d) in
361 the developing resting spores. (e) in actively growing sporogenic plasmodia. (f-h): Localisation of Ec32m vBPO
362 mRNAs (yellow signal) using smFISH. (f) vBPO mRNAs close to sporangia of *M. ectocarpii*. (g, h) vBPO mRNAs
363 inside of *M. ectocarpii* infected cells. arrowheads: early infection, plasmodia containing several nuclei; asterisks:
364 later infection stage, large plasmodia with numerous parasite nuclei. (i, j): Mex1 mRNAs in the cytosol of infected
365 *B. rapa* root cells using smFISH (Red signals, Quasar 570). Mex1 mRNAs are detected near the amyloplasts (black
366 areas). Bars = 10 µm. Images of the controls of these experiments are provided in Suppl. Fig. S4.

367



368

369

370 **Figure 3:** Localisation and quantification of PbBSMT mRNA in *P. brassicae*. a-c: diagrammatic overview of the *P. brassicae*

371 structures seen in the brightfield images (d-e) and the FISH images (g-i). (a) The cell that is fully pictured in (a) shows a plasmodium which is at the onset of spore formation (orange polygon) inside a hypertrophied host cell (cell walls are indicated

372 by the green lines). At the onset of spore formation round, spore like aggregations of the plasmodium become visible (orange circles). During this development stage high numbers of mRNAs can be detected (see image g) which are randomly distributed

373 when no structures are visible in the plasmodium, but appear aggregated around the spore like structures. When the differentiation of the plasmodium progresses (b) these spore like, aggregated areas become more distinct until they have

374 developed into individual resting spores which are not connected via the plasmodium anymore (orange dots). Signals peak

375 around areas which already start to be recognisable as individual portions and get less in areas where resting spores are

376 formed. Finally, the whole plasmodium has developed into resting spores (c, orange dots), that fill the entire host cell. The

377 mRNA signals decrease further in number and brightness before disappearing completely. Bars = 10 μm . (j) Signal maxima

378 μm^{-3} of smFISH PbBSMT signals (n=37) highlighting a peaking of PbBSMT mRNAs during spore formation. Labelling on the x-

379 axes corresponds to the life cycle stages in images (a-c). No significant correlation was identified. One extreme outlier at

380 0.088 signals μm^{-3} is not displayed to improve figure layout.

381

382

383 In addition to the previously reported increase of PbBSMT expression during the later phases
384 of the pathogen life cycle PbBSMT mRNAs could be detected in plasmodia that clearly were
385 in the very early stage of secondary infection (Suppl. Fig. 5). Those plasmodia were very small
386 in size (ca. 20 μm) and the host cells did not yet show the typical hypertrophied phenotype what
387 is typical for cells which house the much larger, actively growing multinucleate plasmodia
388 which can easily reach 100 – 150 μm in size. The young plasmodia in which the PbBSMT
389 mRNAs were detected did also appear to move from one cell to the next (Suppl. Fig. S5, S6).
390 The number of signal maxima per μm^3 was higher with RCA FISH (median $4,47 \times 10^{-02} \pm$
391 RSD $3,01 \times 10^{-02}$ signal maxima μm^{-3} , n=9) than with smFISH (median $9,38 \times 10^{-03} \pm$ RSD
392 $5,26 \times 10^{-02}$ signal maxima μm^3 , n=37 Suppl. Tab. 4). However, when smFISH was used, the
393 number of cells in which signals could be detected was considerably higher and more consistent
394 across different samples. Additionally, the detection efficacy of smFISH was higher: more cells
395 did produce useful results comparing the number of positive cells per image per experiment
396 (Suppl. Fig. S1, S2). Overall the detection efficacy of RCA FISH was lower (ca. 30% positive
397 experiments, n = 16) compared to smFISH (ca. 45% positive experiments, n = 35). Therefore,
398 we concluded that for our pathosystem smFISH is more suitable: the reduced number of signal
399 maxima μm^{-3} are compensated by a 5-10-fold increased number of cells with positive signals
400 and a 15 % higher success rate. For this reason, transcripts of *Brassica oleracea* (MEX1) and
401 *Ectocarpus siliculosus* (vBPO) were analysed with smFISH only.

402

403 **Microscopic analyses**

404 We also compared CLSM and spinning-disk microscopy. Both methods performed very
405 similarly producing complementary mRNA detection patterns (Suppl. Fig. S6). Hand-cutting
406 of clubroot tissue was the best and most reliable method to prepare samples for microscopy
407 (Suppl. Note S1), which resulted in slightly uneven samples. Because of this, CLSM was the
408 method of choice because it better allows to analyse thicker samples than wide field and
409 spinning disk microscopy.

410

411 **Localisation of *P. brassicae* Actin1 by RCA-FISH**

412 The Actin1-gene mRNA was detected in all life cycle stages of *P. brassicae* (Fig. 2c-e, Suppl.
413 Fig S8), as bright, dot-like structures. Signals were spread evenly within cells (Fig. 2c-e) and
414 could be visualised in individual planes (Suppl. Fig. S8 c-d) while in the maximum projection
415 of all optical slices these dots often accumulated to larger signal hotspots (Fig 2c, Suppl. Fig.
416 S8 e, f). In maximum projections, dots were sometimes well separated (Fig 2c) while in other
417 cells the signal was less defined appearing “blurred” and filling most of the cell without clear
418 structural pattern (Fig 2e), indicating areas with multiple mRNA copies. The controls did not
419 show any comparable signals, only a very weak background of autofluorescence was detected
420 (Suppl. Fig. S4 c-e, Fig. S8 a-b).

421

422 **Localisation of plant and algal transcripts during infection by phytomyxids**

423 *Brassica rapa* maltose excess protein 1 (MEX1, smFISH)

424 MEX1 encodes a transporter located in the chloroplast envelope; it is essential for the transport
425 of maltose, the main product of starch breakdown, from the amyloplast to the cytosol (Stettler
426 *et al.*, 2009). MEX1 transcripts were detected as clear dots in the cytosol of the Brassica root

427 cells. Dot-like signals could be observed in root cells containing amyloplasts and which were
428 infected with *P. brassicae* (Fig. 2 i-j). The signal for MEX1 was not present in cells filled with
429 spores and cells that did not contain amyloplasts (Suppl. Fig. S9). Similar to the previously
430 described genes localised detection (“dots”) could be seen in the individual optical slices and
431 the maximum projection images indicating that mRNAs for MEX1 are present in the whole
432 cytosol of the plant. In both controls, the RNase treated samples and the unlabelled infected
433 samples, no characteristic signals were detected (Suppl. Fig. S4 i-j).

434

435 *Ectocarpus siliculosus* vanadium-dependent bromoperoxidase (vBPO, smFISH)

436 mRNA detection in brown algae required adaptations of the protocol. The filamentous growth
437 of *E. siliculosus* and of *M. pyrifera* gametophytes made it necessary to use small tufts of algal
438 material, which are difficult to handle because of their size and shape and do not attach well to
439 Poly L-lysine-coated slides. To reduce the risk of losing the samples, tubes were used to
440 incubate and wash them (see Suppl. Note S1).

441 vBPO has previously been shown to play a role in the response of *Ectocarpus siliculosus* Ec32m
442 against pathogens (Strittmatter *et al.*, 2016) and more generally, in the responses of kelps to
443 elicitors (Cosse *et al.*, 2009). RCA-FISH was tested without success on the algal material (data
444 not shown), but smFISH allowed detection of vBPO mRNAs in Ec32m cells infected with the
445 phytomyxid *Maullinia ectocarpii* (Fig. 2 f-h, Suppl. Fig. S10 g-i). Likewise, signals were
446 detected in *M. ectocarpii* infected *M. pyrifera* cells (Suppl. Fig. S10 a-f). In both cases, signals
447 were dot-like, yet much more confined - than in the plant and phytomyxids tested.

448

449

450 Discussion

451

452 **mRNA localisation is a powerful tool to study pathogen – host interactions**

453 Here, we demonstrate the feasibility of localising mRNA transcripts of phytomyxid pathogens
454 and their plant and algal hosts, which to our knowledge is the first time this method has been
455 used on brown algae, phytomyxids and to analyse biological interactions between two
456 eukaryote species. Localising mRNAs permits the identification and analyses of spatiotemporal
457 pattern of mRNAs in the cytoplasm. Both methods tested (smFISH, RCA-FISH) are very
458 accessible once a gene of interest in biological interactions is identified. Using mRNA FISH
459 allows to overcome important technical bottlenecks that hamper research on important non-
460 model pathogens, plants or algae (Schwelm *et al.*, 2018). Our protocols therefore have huge
461 potential to move our knowledge of these interactions beyond the limitations of RNAseq and
462 organisms for which genetic amendments are possible (Buxbaum *et al.*, 2015). Using clubroots
463 from commercial fields, we directly show the applicability of the methods to investigate host-
464 pathogen interactions in wild type populations and plants grown under natural conditions. The
465 here presented methods will in the coming years greatly increase our understanding of
466 subcellular gene expression pattern, similar to the leap in knowledge that happened in model
467 organisms (Gaspar & Ephrussi, 2015; Lee *et al.*, 2016; Medioni & Besse, 2018).

468 FISH is – as any nucleic acid based method – very adaptable to the needs of the user. A
469 multitude of protocols are available, many of which are variations of the two protocols tested
470 here (reviewed by van Gijtenbeek & Kok, 2017). When selecting the most suitable method a
471 couple of factors need to be kept in mind (Tab. 2). Generally, it can be said that the more
472 complex a biological system, the less complex the method of choice should be: the efficacy for
473 the detection of phytomyxid mRNAs was 15 % higher when the less complex smFISH method
474 was used than with RCA-FISH. On the other hand, smFISH requires mRNAs which are longer
475 than 500 bp to fit a relevant number of probes, while this size restriction does not apply to RCA-
476 FISH. We did prove here that the two contrastingly complex FISH methods can be used to
477 generate meaningful results (Tab. 2).

478 The mRNA signal pattern did differ between plants, brown algae and *P. brassicae* (Fig. 2).
479 Plant mRNAs followed the pattern that were expected based on the pioneering works on
480 smFISH in plants (Duncan *et al.*, 2016b): mRNA signals were dot-like and distributed more or
481 less evenly in cells and were similar in size and shape (Fig. 2i-j, Suppl. Fig. S9). The mRNA
482 pattern in brown algae are comparable to the ones in plants, although signals were somewhat
483 more restricted (Fig. 2f-h, Suppl. Fig. S10). The mRNA pattern observed in phytomyxids are
484 only comparable when few mRNAs are detected in the plasmodia (e.g. Fig 2b). However, when
485 many mRNAs are present close to each other the individual mRNAs do not resolve and are
486 displayed as larger areas, especially in the maximum projections of the z-stacks (Fig. 2, Fig 3).
487 Although phytomyxid plasmodia are similar in size and shape to their host cell (Fig. 3), each
488 plasmodium has to be interpreted as an aggregation of hundreds to thousands small cells with
489 an individual diameter of 3-5 μm and each with its own nucleus (compare e.g. Fig 2b insert, or
490 Fig 2 f-h). So the space which can be populated by mRNAs is much more confined than in the
491 comparably gargantuan host cells. This is visually amplified in maximum projections of z-
492 stacks, because one plasmodium contains more than one layer of cells (one layer per 3-5 μm).

493 It is, however, very important to note that these technical and biological limitations are clearly
 494 counterbalanced by the amount of biological information that can be gathered.

495
 496

497 **Table 2: Advantages and disadvantages of RCA-FISH and smFISH.** Prices can vary and are estimates based
 498 on Austrian prices 2017 including 20 % VAT.

	RCA FISH	smFISH
Pros	<ul style="list-style-type: none"> ▪ Signal amplification in theory allows to monitor single copy mRNAs also in samples with a high fluorescent background. ▪ Specificity: Highly specific probes can be designed to distinguish between paralogues or SNPs . ▪ No gene length limitation: short (<500 bp) genes can be analysed. ▪ Modular: Possibility of combination with in situ proximity ligation assays to collect information on mRNA-protein interactions or post-translational modification (not tested in the scope of this paper). 	<ul style="list-style-type: none"> ▪ Signal amplification in theory allows to monitor single copy mRNAs in samples with a high fluorescent background. ▪ Complexity: easy probe design, few steps minimising contamination risks. ▪ Cell permeability: small probes, no large functional molecules involved. ▪ Cost of reagents: most reagents needed are standard lab consumables. ▪ Time: Fast protocol, ca. 1 day from sample to image, hands on time ca 3 h.
Cons	<ul style="list-style-type: none"> ▪ Complexity: many steps increase the risk of RNase contamination or errors. ▪ Cell permeability: Involves multiple steps requiring large enzymes which need to reach the cytoplasm. This is a major drawback for use in the plant/algal system. ▪ Costs of probes: The expensive LNA- and Padlock probes need to be designed for each gene (ca. 400€ per gene for ~200 reactions). ▪ Costs of reagents: pricey reagents and enzymes are used (ca 75€ per reaction). ▪ Time: ca. 2 days from sample to image, of which there are ca 6 h hands on time. 	<ul style="list-style-type: none"> ▪ Specificity: using standard FISH probes in a “string of beads” manner opens possibility of false positives for isoforms, orthologues or conserved gene families. ▪ Gene length limitation: Short mRNA sequences (< 500 bp) are not suitable for smFISH. ▪ Costs of probes: 24-48 labelled probes are needed for each gene. Some companies offer discounts on smFISH probes (ca. 500-800€ depending on the number of probes and the fluorophore, ~1000+ reactions).

499
 500
 501
 502
 503
 504

505 **RNA stability and accessibility are crucial – or how do you get the protocol to work?**

506 Here we show that both smFISH and RCA-FISH methods are suitable for *in situ* mRNA
507 monitoring in the host and the pathogen. While analysing three totally different biological
508 systems (plants, algae, phytomyxids) it became clear that the overall success and efficiency of
509 the method is determined by the fixation of the mRNAs in the sample material and the
510 permeability of the cell walls, both factors that differ across organisms. Fixation methods and
511 the duration of storage post-fixation influenced the number of cells in which signals could be
512 detected; however, this was different across sample types and genes so no clear maximum or
513 minimum duration of storage could be established. Since decreasing signal intensities can be
514 caused by RNA degradation during storage, we recommend to use the samples as soon as
515 possible after harvesting. However, we found that samples kept in an RNase-free environment
516 give good results after more than one year. Another reason for decreasing signals can be
517 formaldehyde mediated covalent interlinking of mRNAs and the RNA-binding proteins which
518 are responsible for the transport of the RNA to the site of translation (Foley *et al.*, 2017;
519 Niessing *et al.*, 2018), or mRNA secondary structures that do not permit the binding of the
520 probes to the sites of interest (Ding *et al.*, 2013). Because of this, we recommend not to store
521 the samples in the formaldehyde containing fixative, but to move them to pure ethanol for long
522 term storage. RNA-binding proteins and mRNA secondary structure can impact on the success
523 of the detection method without the fixation bias mentioned above, because both can limit the
524 accessibility of the target site for probes (Foley *et al.*, 2017).

525 On the other hand, the permeability of cell walls and plant tissue as a whole is a constraint for
526 FISH-based methods. In this study, RCA-FISH was not adaptable to study interactions in
527 filamentous algae, most likely because the enzymes needed could not permeate the cell walls.
528 Cutting of the algae without destruction of the cell arrangement is very difficult and usually
529 cutting of the algae results in a loss of spatial information. All tested permeabilisation efforts
530 did not improve the signal yield. Also in plants the efficacy of the mRNA detection was lower
531 in RCA-FISH, as signals were only visible in cells which were cut open, but never in cells with
532 an intact cell wall. The cooperatively small probes used for smFISH could be used on all
533 samples without additional permeabilisation steps.

534

535 **mRNA localisation sheds light on phytomyxid biology**

536 In this study, we determined the expression and localisation pattern of three pathogen genes,
537 one plant and one brown algal gene. All mRNAs chosen had a putative function assigned to
538 pre-existing information on the expected expression pattern. However, the single cell resolution
539 of our experiments resulted in information, which is already improving our understanding of
540 the biological interaction. These findings also showcase the potential gain of using mRNA FISH
541 to advance our knowledge on plant pathogen interactions beyond the state of the art.

542 Biologically most interesting was the expression pattern of PbBSMT, a SABATH-type
543 methyltransferase produced by *P. brassicae*. This methyltransferase has structural similarities
544 to plant methyltransferases. Previous qPCR analysis of its expression pattern showed, that its
545 expression during clubroot development is highest when the concentration of SA in the roots
546 peaks, which is the reason why a role in disease development of this gene has been discussed
547 (Ludwig-Muller *et al.*, 2015; Bulman *et al.*, 2018). In our in-situ experiments, PbBSMT
548 mRNAs started to appear in small developing plasmodia (Suppl. Fig S5, S6). Small amounts of

549 PbBSMT have been detected previously during early infection in EST (expressed sequence tag)
550 libraries (Bulman *et al.*, 2006) and callus culture transcriptome analyses (Bulman *et al.*, 2011).
551 We observed mRNAs of PbBSMT in small plasmodia which appear to move from cell to cell
552 (Suppl. Fig. S6). There is anecdotal evidence that plasmodia can move from cell to cell using
553 cell wall breaks or plasmodesmata (Donald *et al.*, 2008; Riascos *et al.*, 2011), but our results
554 are the first to show that this movement is linked with the expression of a putative effector that
555 alters the host defence.

556 Using FISH we clearly demonstrate, that PbBSMT mRNAs start to increase when *P. brassicae*
557 transitions from plasmodial growth to spore formation. The detected mRNAs peaked when
558 young, immature resting spores became recognisable (Fig 3). These results again confirm
559 findings from previous studies (Ludwig-Muller *et al.*, 2015; Bulman *et al.*, 2018), but our
560 results are the first to pinpoint these changes to specific life cycle stages. Notably PbBSMT
561 mRNAs accumulate around the developing resting spores in the sporogenic plasmodia (Fig. 3,
562 Suppl. Video 1). This accumulation of PbBSMT mRNAs around the developing resting spores
563 is striking, because during spore formation chitin is produced. The here presented results
564 therefore reinforce the previously established hypothesis that PbBSMT is produced to inactivate
565 SA produced by the host in response to chitin (Ludwig-Müller *et al.*, 2015; Schwelm *et al.*,
566 2015). *P. brassicae* resting spores contain chitin in their cell wall (Cavalier-Smith & Chao,
567 2003), which is one of the best studied elicitors of plant defence and induces (amongst others)
568 SA production (Fesel & Zuccaro, 2016). On the other hand, methylsalicylate is a more volatile
569 and membrane-permeable form of SA and is either excreted via the leaves or an inducer of
570 systemic responses in plants (Vlot *et al.*, 2017). Combined with findings from previous studies
571 (Ludwig-Muller *et al.*, 2015; Bulman *et al.*, 2018), our observations strongly support the role
572 in host defence suppression of PbBSMT, making it a very interesting target for future studies.

573 With the here presented methods we could confirm a direct interaction and interference of
574 phytomyxids on the transcriptional status of infected cells. Roots of brassicas infected with *P.*
575 *brassicae* show a marked accumulation of starch (Ludwig-Müller *et al.*, 2009). MEX1, a gene
576 coding for a maltose transporter essential for transporting maltose from the amyloplast to the
577 cytosol (Stettler *et al.*, 2009). With smFISH we could localise MEX1 mRNAs in plant cells
578 containing amyloplasts and plasmodia of *P. brassicae* (Suppl. Fig. S9). The presence of
579 mRNAs is an indicator of ongoing synthesis of a host protein, because of the short half live of
580 mRNAs in vivo (Merchante *et al.*, 2017). Therefore, it is likely that MEX1 is activated by
581 growing *P. brassicae* plasmodia to mediate energy supply from the host to the pathogen.

582 The brown algal vBPO has previously been linked to stress response (Leblanc *et al.*, 2015;
583 Strittmatter *et al.*, 2016). Here we could confirm that vBPO mRNAs are located in *E. siliculosus*
584 and *M. pyrifera* cells, which show early infections with *Maullinia ectocarpii*, while in cells
585 where the infection has advanced to sporangial development no signals were identified. This
586 confirms that brown algae, like plants, show a localised stress response to plasmodiophorid
587 pathogens. Whether or not this type of stress response is a general pattern in brown algae or if
588 this is specific for infections with phytomyxids was beyond the scope of this study.

589

590

591 **Acknowledgements**

592 JB and SN were funded by the Austrian Science Fund (FWF): grant Y801-B16 (START-grant).
593 CG has received funding from the European Union's Horizon 2020 research and innovation
594 programme under the Marie Skłodowska-Curie grant agreement No 642575, and from the UK
595 NERC under the grant agreement GlobalSeaweed (NE/L013223/1). We thank Stefan Ciaghi
596 for providing the transcriptomic data for MEX1. The authors want to thank Martin Kirchmair,
597 Arne Schwelm, Mohammad Etemadi and Stefan Ciaghi for useful discussions.

598

599 **Author Contribution and References**

600 JB and SN designed the research, collected, analysed and interpreted data and wrote the
601 manuscript with feedback from all co-authors; JB performed the research; CG provided algal
602 material and algal data; AMS analysed the images. All authors read and contributed to the final
603 MS.

604

605

606 **Archibald JM, Keeling PJ. 2004.** Actin and Ubiquitin Protein Sequences Support a
607 Cercozoan/Foraminiferan Ancestry for the Plasmodiophorid Plant Pathogens. *Journal of*
608 *Eukaryotic Microbiology* **51**(1): 113-118.

609 **Bruno L, Muto A, Spadafora ND, Iaria D, Chiappetta A, Van Lijsebettens M, Bitonti MB. 2011.** Multi-
610 probe in situ hybridization to whole mount Arabidopsis seedlings. *International Journal of*
611 *Developmental Biology* **55**(2): 197-203.

612 **Bulman S, Candy JM, Fiers M, Lister R, Conner AJ, Eady CC. 2011.** Genomics of Biotrophic, Plant-
613 infecting Plasmodiophorids Using In Vitro Dual Cultures. *Protist* **162**(3): 449-461.

614 **Bulman S, Richter F, Marschollek S, Benade F, Jülke S, Ludwig-Müller J. 2018.** Arabidopsis thaliana
615 expressing PbBSMT, a gene encoding a SABATH-type methyltransferase from the plant
616 pathogenic protist Plasmodiophora brassicae, show leaf chlorosis and altered host
617 susceptibility. *Plant biology (Stuttgart, Germany)*.

618 **Bulman S, Siemens J, Ridgway HJ, Eady C, Conner AJ. 2006.** Identification of genes from the obligate
619 intracellular plant pathogen, Plasmodiophora brassicae. *Fems Microbiology Letters* **264**(2):
620 198-204.

621 **Buxbaum AR, Haimovich G, Singer RH. 2015.** In the right place at the right time: visualizing and
622 understanding mRNA localization. *Nature Reviews Molecular Cell Biology* **16**(2): 95-109.

623 **Cavalier-Smith T, Chao EEY. 2003.** Phylogeny of choanozoa, apusozoa, and other protozoa and early
624 eukaryote megaevolution. *Journal of Molecular Evolution* **56**(5): 540-563.

625 **Chen KH, Boettiger AN, Moffitt JR, Wang SY, Zhuang XW. 2015.** Spatially resolved, highly multiplexed
626 RNA profiling in single cells. *Science* **348**(6233).

627 **Cormier A, Avia K, Sterck L, Derrien T, Wucher V, Andres G, Monsoor M, Godfroy O, Lipinska A,
628 Perrineau MM, et al. 2016.** Re-annotation, improved large-scale assembly and establishment
629 of a catalogue of noncoding loci for the genome of the model brown alga Ectocarpus. *New*
630 *Phytologist* **214**(1): 219-232.

631 **Cosse A, Potin P, Leblanc C. 2009.** Patterns of gene expression induced by oligoguluronates reveal
632 conserved and environment-specific molecular defense responses in the brown alga Laminaria
633 digitata. *New Phytologist* **182**(1): 239-250.

634 **Ding Y, Tang Y, Kwok CK, Zhang Y, Bevilacqua PC, Assmann SM. 2013.** In vivo genome-wide profiling
635 of RNA secondary structure reveals novel regulatory features. *Nature* **505**: 696.

- 636 **Donald EC, Jaudzems G, Porter IJ. 2008.** Pathology of cortical invasion by *Plasmodiophora brassicae* in
637 clubroot resistant and susceptible *Brassica oleracea* hosts. *Plant Pathology* **57**(2): 201-209.
- 638 **Duncan S, Olsson TSG, Hartley M, Dean C, Rosa S. 2016a.** A method for detecting single mRNA
639 molecules in *Arabidopsis thaliana*. *Plant Methods* **12**: 13.
- 640 **Duncan S, Olsson TSG, Hartley M, Dean C, Rosa S. 2016b.** A method for detecting single mRNA
641 molecules in *Arabidopsis thaliana*. *Plant Methods* **12**.
- 642 **Egan S, Harder T, Burke C, Steinberg P, Kjelleberg S, Thomas T. 2013.** The seaweed holobiont:
643 understanding seaweed–bacteria interactions. *Fems Microbiology Reviews* **37**(3): 462-476.
- 644 **Farnham G, Strittmatter M, Coelho S, Cock JM, Brownlee C. 2013.** Gene silencing in *Fucus* embryos:
645 developmental consequences of RNAi-mediated cytoskeletal disruption. *J Phycol* **49**(5): 819-
646 829.
- 647 **Fesel PH, Zuccaro A. 2016.** beta-glucan: Crucial component of the fungal cell wall and elusive MAMP
648 in plants. *Fungal Genetics and Biology* **90**: 53-60.
- 649 **Foley SW, Kramer MC, Gregory BD. 2017.** RNA structure, binding, and coordination in *Arabidopsis*.
650 *Wiley Interdisciplinary Reviews: RNA* **8**(5): e1426.
- 651 **Francoz E, Ranocha P, Pernot C, Le Ru A, Pacquit V, Dunand C, Burlat V. 2016.** Complementarity of
652 medium-throughput in situ RNA hybridization and tissue-specific transcriptomics: case study
653 of *Arabidopsis* seed development kinetics. *Scientific Reports* **6**.
- 654 **Gaspar I, Ephrussi A. 2015.** Strength in numbers: quantitative single-molecule RNA detection assays.
655 *Wiley Interdisciplinary Reviews: Developmental Biology* **4**(2): 135-150.
- 656 **Irani S, Trost B, Waldner M, Nayidu N, Tu J, Kusalik AJ, Todd CD, Wei Y, Bonham-Smith PC. 2018.**
657 Transcriptome analysis of response to *Plasmodiophora brassicae* infection in the *Arabidopsis*
658 shoot and root. *BMC genomics* **19**(1): 23.
- 659 **Kemen E, Jones JDG. 2012.** Obligate biotroph parasitism: can we link genomes to lifestyles? *Trends in*
660 *Plant Science* **17**(8): 448-457.
- 661 **Leblanc C, Vilter H, Fournier JB, Delage L, Potin P, Rebuffet E, Michel G, Solari PL, Feiters MC, Czjzek**
662 **M. 2015.** Vanadium haloperoxidases: From the discovery 30 years ago to X-ray crystallographic
663 and V K-edge absorption spectroscopic studies. *Coordination Chemistry Reviews* **301**: 134-146.
- 664 **Lee C, Roberts SE, Gladfelter AS. 2016.** Quantitative spatial analysis of transcripts in multinucleate cells
665 using single-molecule FISH. *Methods* **98**: 124-133.
- 666 **Libault M, Pingault L, Zogli P, Schiefelbein J. 2017.** Plant Systems Biology at the Single-Cell Level.
667 *Trends in Plant Science* **22**(11): 949-960.
- 668 **Ludwig-Muller J, Julke S, Geiss K, Richter F, Mithofer A, Sola I, Rusak G, Keenan S, Bulman S. 2015.** A
669 novel methyltransferase from the intracellular pathogen *Plasmodiophora brassicae*
670 methylates salicylic acid. *Mol Plant Pathol* **16**(4): 349-364.
- 671 **Ludwig-Müller J, Prinsen E, Rolfe SA, Scholes JD. 2009.** Metabolism and plant hormone action during
672 clubroot disease. *Journal of Plant Growth Regulation* **28**(3): 229-244.
- 673 **Ludwig-Müller J, Jülke S, Geiß K, Richter F, Mithöfer A, Šola I, Rusak G, Keenan S, Bulman S. 2015.** A
674 novel methyltransferase from the intracellular pathogen *Plasmodiophora brassicae*
675 methylates salicylic acid. *Molecular Plant Pathology* **16**(4): 349-364.
- 676 **Maier I, Parodi E, Westermeier R, Muller DG. 2000.** *Maullinia ectocarpii* gen. et sp. nov.
677 (*Plasmodiophorea*), an intracellular parasite in *Ectocarpus siliculosus* (*Ectocarpales*,
678 *Phaeophyceae*) and other filamentous brown algae. *Protist* **151**(3): 225-238.
- 679 **Medioni C, Besse F. 2018.** The Secret Life of RNA: Lessons from Emerging Methodologies. In: Gaspar I
680 ed. *RNA Detection: Methods and Protocols*. New York, NY: Springer New York, 1-28.

- 681 **Merchante C, Stepanova AN, Alonso JM. 2017.** Translation regulation in plants: an interesting past,
682 an exciting present and a promising future. *The Plant Journal* **90**(4): 628-653.
- 683 **Misra BB, Assmann SM, Chen SX. 2014.** Plant single-cell and single-cell-type metabolomics. *Trends in*
684 *Plant Science* **19**(10): 637-646.
- 685 **Moor AE, Itzkovitz S. 2017.** Spatial transcriptomics: paving the way for tissue-level systems biology.
686 *Current Opinion in Biotechnology* **46**: 126-133.
- 687 **Müller DB, Vogel C, Bai Y, Vorholt JA. 2016.** The Plant Microbiota: Systems-Level Insights and
688 Perspectives. *Annual Review of Genetics* **50**(1): 211-234.
- 689 **Murúa P, Goecke F, Westermeier R, van West P, Kupper FC, Neuhauser S. 2017.** *Mauullinia braseltonii*
690 sp nov (Rhizaria, Phytomyxea, Phagomyxida): A Cyst-forming Parasite of the Bull Kelp
691 *Durvillaea* spp. (Stramenopila, Phaeophyceae, Fucales). *Protist* **168**(4): 468-480.
- 692 **Neuhauser S, Huber L, Kirchmair M. 2011.** Is *Roesleria subterranea* a primary pathogen or a minor
693 parasite of grapevines? Risk assessment and a diagnostic decision scheme. *European Journal*
694 *of Plant Pathology* **130**(4): 503-510.
- 695 **Niessing D, Jansen RP, Pohlmann T, Feldbrugge M. 2018.** mRNA transport in fungal top models. *Wiley*
696 *Interdisciplinary Reviews-Rna* **9**(1).
- 697 **Riascos D, Ortiz E, Quintero D, Montoya L, Hoyos-Carvajal L. 2011.** Histopathological and
698 morphological alterations caused by plasmodiophora brassicae in brassica oleracea
699 *Agronomía Colombiana* **29**: 57-67.
- 700 **Rolfe SA, Strelkov SE, Links MG, Clarke WE, Robinson SJ, Djavaheri M, Malinowski R, Haddadi P,**
701 **Kagale S, Parkin IA. 2016.** The compact genome of the plant pathogen *Plasmodiophora*
702 *brassicae* is adapted to intracellular interactions with host *Brassica* spp. *BMC genomics* **17**(1):
703 272.
- 704 **Schneider CA, Rasband WS, Eliceiri KW. 2012.** NIH Image to ImageJ: 25 years of image analysis. *Nature*
705 *Methods* **9**: 671.
- 706 **Schwelm A, Badstober J, Bulman S, Desoignies N, Etemadi M, Falloon RE, Gachon CMM, Legreve A,**
707 **Lukes J, Merz U, et al. 2018.** Not in your usual Top 10: protists that infect plants and algae.
708 *Mol Plant Pathol* **19**(4): 1029-1044.
- 709 **Schwelm A, Fogelqvist J, Knaust A, Jülke S, Lilja T, Bonilla-Rosso G, Karlsson M, Shevchenko A,**
710 **Dhandapani V, Choi SR. 2015.** The *Plasmodiophora brassicae* genome reveals insights in its life
711 cycle and ancestry of chitin synthases. *Scientific Reports* **5**: 11153.
- 712 **Singh K, Tzelepis G, Zouhar M, Ryšánek P, Dixelius C. 2018.** The immunophilin repertoire of
713 *Plasmodiophora brassicae* and functional analysis of PbCYP3 cyclophilin. *Molecular Genetics*
714 *and Genomics* **293**(2): 381-390.
- 715 **Stettler M, Eicke S, Mettler T, Messerli G, Hortensteiner S, Zeeman SC. 2009.** Blocking the metabolism
716 of starch breakdown products in *Arabidopsis* leaves triggers chloroplast degradation. *Mol*
717 *Plant* **2**(6): 1233-1246.
- 718 **Strittmatter M, Grenville-Briggs LJ, Breithut L, Van West P, Gachon CM, Kupper FC. 2016.** Infection of
719 the brown alga *Ectocarpus siliculosus* by the oomycete *Eurychasma dicksonii* induces oxidative
720 stress and halogen metabolism. *Plant Cell Environ* **39**(2): 259-271.
- 721 **Trcek T, Lionnet T, Shroff H, Lehmann R. 2017.** mRNA quantification using single-molecule FISH in
722 *Drosophila* embryos. *Nature Protocols* **12**(7): 1326-1348.
- 723 **van Gijtenbeek LA, Kok J. 2017.** Illuminating Messengers: An Update and Outlook on RNA Visualization
724 in Bacteria. *Frontiers in Microbiology* **8**: 1-19.
- 725 **Vandenkoornhuysse P, Quaiser A, Duhamel M, Le Van A, Dufresne A. 2015.** The importance of the
726 microbiome of the plant holobiont. *New Phytologist* **206**(4): 1196-1206.

- 727 **Vlot AC, Pabst E, Riedlmeier M. 2017.** Systemic Signalling in Plant Defence. *eLS*.
- 728 **Wang DJ, Bodovitz S. 2010.** Single cell analysis: the new frontier in 'omics'. *Trends in Biotechnology*
- 729 **28(6): 281-290.**
- 730 **Weibrecht I, Lundin E, Kiflemariam S, Mignardi M, Grundberg I, Larsson C, Koos B, Nilsson M,**
- 731 **Soderberg O. 2013.** In situ detection of individual mRNA molecules and protein complexes or
- 732 post-translational modifications using padlock probes combined with the in situ proximity
- 733 ligation assay. *Nat Protoc* **8(2): 355-372.**
- 734 **Weibrecht I, Lundin E, Kiflemariam S, Mignardi M, Grundberg I, Larsson C, Koos B, Nilsson M,**
- 735 **Söderberg O. 2013.** In situ detection of individual mRNA molecules and protein complexes or
- 736 post-translational modifications using padlock probes combined with the in situ proximity
- 737 ligation assay. *Nat. Protocols* **8(2): 355-372.**
- 738 **West JA, McBride DL. 1999.** Long-term and diurnal carpospore discharge patterns in the Ceramiaceae,
- 739 Rhodomelaceae and Delesseriaceae (Rhodophyta). *Hydrobiologia* **398(0): 101-114.**
- 740 **Ye N, Zhang X, Miao M, Fan X, Zheng Y, Xu D, Wang J, Zhou L, Wang D, Gao Y, et al. 2015.** Saccharina
- 741 genomes provide novel insight into kelp biology. *Nature Communications* **6: 6986.**
- 742 **Zeilinger S, Gupta VK, Dahms TES, Silva RN, Singh HB, Upadhyay RS, Gomes EV, Tsui CKM, Nayak SC,**
- 743 **van der Meer JR. 2016.** Friends or foes? Emerging insights from fungal interactions with plants.
- 744 *Fems Microbiology Reviews* **40(2): 182-207.**
- 745
- 746